

Combining 3D Magnetic Force Actuator and Multi-Functional Fluorescence Imaging to Study Nucleus Mechanobiology

Miao Huang^{1,5}, Heyang Wang^{1,5}, Alfredo A. Delgado¹, Tyler A. Reid¹, Julian Long², Shu Wang^{3,5}, Hayley Sussman⁴, Juan Guan^{5,6,7}, Hitomi Yamaguchi¹, Xin Tang^{1,5,8,9}

¹ Department of Mechanical and Aerospace Engineering, Herbert Wertheim College of Engineering, University of Florida ² Department of Materials Science and Engineering, University of Florida ³ Department of Biostatistics, University of Florida ⁴ Department of Biomedical Engineering, College of Engineering (COE), University of Delaware (UD) ⁵ UF Health Cancer Center, University of Florida ⁶ Department of Physics, College of Liberal Arts and Sciences, University of Florida ⁷ Department of Anatomy and Cell Biology, College of Medicine, University of Florida ⁸ J. Crayton Pruitt Family Department of Biomedical Engineering, University of Florida ⁹ Department of Physiology and Functional Genomics, University of Florida

Corresponding Author

Xin Tang xin.tang@ufl.edu

Citation

Huang, M., Wang, H., Delgado, A.A., Reid, T.A., Long, J., Wang, S., Sussman, H., Guan, J., Yamaguchi, H., Tang, X. Combining 3D Magnetic Force Actuator and Multi-Functional Fluorescence Imaging to Study Nucleus Mechanobiology. *J. Vis. Exp.* (185), e64098, doi:10.3791/64098 (2022).

Date Published

July 5, 2022

DOI

10.3791/64098

URL

jove.com/video/64098

Abstract

A fundamental question in mechanobiology is how living cells sense extracellular mechanical stimuli in the context of cell physiology and pathology. The cellular mechano-sensation of extracellular mechanical stimuli is believed to be through the membrane receptors, the associated protein complex, and the cytoskeleton. Recent advances in mechanobiology demonstrate that the cell nucleus in cytoplasm itself can independently sense mechanical stimuli simultaneously. However, a mechanistic understanding of how the cell nucleus senses, transduces, and responds to mechanical stimuli is lacking, mainly because of the technical challenges in accessing and quantifying the nucleus mechanics by conventional tools. This paper describes the design, fabrication, and implementation of a new magnetic force actuator that applies precise and non-invasive 3D mechanical stimuli to directly deform the cell nucleus. Using CRISPR/Cas9-engineered cells, this study demonstrates that this tool, combined with high-resolution confocal fluorescent imaging, enables the revelation of the real-time dynamics of a mechano-sensitive yes-associated protein (YAP) in single cells as a function of nucleus deformation. This simple method has the potential to bridge the current technology gap in the mechanobiology community and provide answers to the knowledge gap that exists in the relation between nucleus mechanotransduction and cell function.



Introduction

This study aims develop to and apply a new technique to elucidate nucleus mechanobiology by combining the magnetic actuators that apply mechanical force directly on the cell nucleus and the confocal fluorescence microscopy that simultaneously images the structural and functional subcellular changes. sense extracellular biophysical signals including tissue stiffness^{1,2,3,4}, interstitial fluid pressure and shear stress^{5,6,7}, surface topology/geometry^{8,9,10,11,12}, and tension/compression stress 13, 14, 15, 16. Biophysical signals are converted into biochemical signals and trigger potential downstream changes of gene expression and cell behaviors-a process known as mechanotransduction 17, 18, 19, 20, 21, 22, 23, 24, 25, 26, 27 study mechanotransduction processes, a myriad of techniques have been developed to apply mechanical force on the cells, such as atomic force microscopy²⁸. cell stretching device²⁹, bio-MEMS (micro-electromechanical systems) force sensor 15,30,31, shear rheology 32, and Stereo Vision System³³. A recent review summarizes the approaches to apply extracellular mechanical cues and interfere with mechanosensing³⁴. To date, most of these methods apply force on the cell plasma membrane, and cells directly receive these extracellular biophysical signals via membrane receptors such as integrin, cadherin, ion channels, and G-Protein-coupled receptors. Subsequently, they transmit the signal to the intracellular cytoskeleton and nucleus. For example, using yes-associated protein (YAP) translocation as an indicator of mechano-sensing, cells are shown to sense the mechanical signals of substrate stiffness and extracellular tension from the cell membrane and transmit them through the cytoskeleton into the nucleus to induce YAP cytoplasm-to-nucleus translocation^{28,35}.

Recent evidence suggests that the cell nucleus itself is an independent mechano-sensor^{8,36,37}. This is proven by experiments performed on the isolated nucleus harvested from cells, where it was revealed that nuclei adaptively change their stiffness in response to the mechanical force directly applied on them³⁶. During many physiological conditions, nuclei in both tumor and healthy cells sense extracellular biophysical signals and change their mechanical properties and assemblies^{38,39,40}. For example, upon extravasation, the nuclear stiffness of tumor cells decreases and maintains softness for over 24 h³⁸. During migration through confined interstitial space, the nuclei of tumor cells frequently lose and recover their structural integrity³⁹. However, the way in which the nucleus senses the biophysical signal is unknown, although several nuclearenvelope proteins and families of proteins have been found to be involved, such as Lamin A/C and linker of nucleoskeleton and cytoskeleton (LINC) complex^{38,41}. Hence, new noninvasive methods that can directly apply force to the nucleus will decouple the effect of force transmission from the cellplasma membrane and cytoskeleton, and will help elucidate the previously inaccessible molecular mechanisms of nuclear mechano-sensing.

Research that employed optical tweezers to manipulate organelles⁴² and microbeads injected into cells⁴³ showed the technological capability of directly applying force on the nucleus. However, the optical-tweezer technique has several limitations: (1) low throughput-optical tweezers often only manipulate one cell or microbead at a time; and (2)



potential photodamage and temperature artifact-deformation of nuclear requires tens of pN^{36} , and the corresponding necessary laser power is about 10 mW per $pN^{44,45}$. Such laser intensity is sufficient to trigger photodamage in the cells and perturb cell functions during the experiment⁴⁶.

Magnetic force applied through microbeads within living cells shows the potential to directly apply force on the nucleus and overcomes the limitations of optical tweezers. Once microbeads are delivered into the cytoplasm, a magnetic field can exert a magnetic force on multiple microbeads simultaneously in a high-throughput manner. The magnetic field does not influence cell functions⁴⁷, but generates force from pN to nN, which is enough to induce nuclear deformation^{36,48,49}. To date, manipulation of magnetic microbeads has been applied on cell plasma membrane⁴⁸, inside the cytoplasm⁵⁰, on F-actin⁵¹, inside the nucleus⁴⁷, and on the isolated nucleus³⁶. However, magnetic manipulation of microbeads has never been used to apply direct mechanical force on the nuclear envelope to study mechanotransduction in the nucleus.

In this paper, a simple technique is developed to non-invasively deliver magnetic microbeads into the cytoplasm and use these microbeads to apply mechanical force on the nucleus (**Figure 1**). Here, CRISPR/Cas9-engineered human normal B2B cell lines that endogenously express mNeonGreen2_{1-10/11}-tagged YAP are used to validate the method. YAP is a mechano-sensitive protein, and the translocation of YAP is regulated by nuclear mechano-sensing^{14,28}. The CRISPR/Cas9-regulated knockin approach was chosen to tag endogenous YAP with a fluorescent protein (FP) mNeonGreen2_{1-10/11}. Although CRISPR editing is known to have incomplete efficiency and off-target effect, the protocols in previous publications

integrated fluorescence sorting to select for correct open reading frame insertion 52,53,54. With this additional layer of selection, no off-target tagging event was observed in 20+ cell lines previously generated 52,53,54,55. This is a split fluorescent protein construct, but in principle, any expressible fluorescent tag could be usable. This labeling approach is superior to transgene or antibody methods. First, unlike the transgene expression, the tagged protein maintains single-copy gene dosage and expresses in the physiological context of the native gene regulatory network, limiting deviations in protein concentration, localization, and interaction. The tagging method used in this study achieves over an order-of-magnitude higher throughput and efficiency than full FP tagging. It also avoids challenges associated with immunofluorescence due to fixation artifacts and the limited availability of high-quality, high-specificity antibodies. Second, the approach used in this paper does minimum perturbation to the cell physiology and enables the realtime revelation of all endogenous YAPs authentically. In contrast, other common transgene methods often lead to overexpression of YAP. The resulting artificial distribution can potentially cause cytotoxicity and affect mechano-sensing of $cells^{56,57,58}$.

This study presents a protocol to directly apply force on the nucleus through magnetic microbeads delivered into the cytoplasm and to conduct simultaneous live-cell fluorescent imaging. In summary, the protocols presented here demonstrate how to (1) deliver magnetic microbeads into the cell while outside the nucleus, (2) manipulate the microbeads to apply magnetic force on the nucleus, (3) perform confocal fluorescent imaging of the cells during manipulation, and (4) quantitatively analyze the YAP nuclear/cytoplasm (N/C) ratio throughout the force application process. The results suggest that (1) through endocytosis,



magnetic microbeads can be non-invasively delivered into the cytoplasm of B2B cells within 7 h (**Figure 2** and **Figure 3**); and (2) quantified magnetic force directly applied on the nucleus (**Figure 4**, **Figure 5**, and **Figure 6**) alone can trigger diverse changes of YAP N/C ratio in CRISPR/Cas9-engineered B2B cells (**Figure 7** and **Figure 8**).

Protocol

1. Maintenance of CRISPR/Cas9-engineered B2B cells

- Culture B2B cells in a T25 flask with RPMI-1640 supplemented with 10% fetal bovine serum and 1% penicillin-streptomycin.
- Maintain the B2B cells in a humidified incubator at 37 °C with 5% CO₂.
- 3. Subculture the B2B cells when the confluency reaches 70% to 80%.
- 4. Store the B2B cell line in RPMI-1640 culture medium with 10% (v/v) DMSO in a -80 °C freezer.
- Use the B2B cells with a passage number less than 10 in the experiments.

2. Cell culture

- Seed the cells onto a glass-bottom Petri dish.
 - Move the flask that contains B2B cells inside from the incubator to the biosafety cabinet.
 - Remove the culture medium in the flask using an aspirating pipette with a vacuum pump connected.
 - Wash the flask with 2 mL of phosphate-buffered saline (PBS).
 - 4. Remove PBS using the aspirating pipette.

- Add 0.5 mL of 0.05% Trypsin solution to detach cells from the bottom of the flask substrate.
- 6. Put the flask in the incubator for 5 min.
- Move the flask to the biosafety cabinet. Add 5 mL of new culture medium into the flask and pipette the solution up and down.
- Deposit 50 μL of the medium with cells (300 cells/μL)
 onto the glass-bottom Petri dish. Add 2 mL of culture
 medium into the Petri dish.
- Place the Petri dish into the incubator. Wait for 12 h for the cells to attach.
- 2. Culture the cells with magnetic microbeads.
 - Weigh 0.2 g of 7 μm mean diameter carbonyl iron microbeads (hereafter called 7 μm microbeads, see the Table of Materials).
 - Use a pipette to suspend the microbeads in 1 mL of RPMI-1640 culture medium.
 - Take the Petri dish with B2B cells to the biosafety cabinet.
 - Add 200 μL of the medium containing microbeads into the Petri dish.
 - NOTE: Add the medium quickly to avoid precipitation of the microbeads.
 - Put the Petri dish back in the incubator until microbeads are internalized by the cells. Check the internalization every 6 h to determine the optimal time for internalization for different cell lines.
 - To check the internalization, perform confocal fluorescence imaging to visualize the microbead, nuclear, and cell boundary. If the microbead is



internalized by the cell, it will be within the cell boundary.

3. Visualization of nucleus

- Warm 1.5 mL of the culture medium in the incubator for 15 min.
- Turn off the light of the biosafety cabinet. Take the Petri dish that contains the cell, warmed culture medium, nuclear stain, and Verapamil HCl into the biosafety cabinet.

NOTE: Nuclear staining components are sensitive to light. Avoid exposure to light during operation.

- 3. Dilute 1000x nuclear stain by DMSO to 100x.
- 4. Dilute 100 mM Verapamil HCl by DMSO to 10 mM.
- Add 15 μL of 100x nuclear stain and 15 μL of 10 mM
 Verapamil HCl to 1.5 mL of culture medium. Mix well by pipetting up and down.
- Remove the culture medium from the Petri dish. Add the culture medium containing nuclear staining into the Petri dish.
- Put the cells back in the incubator for over 2 h.

4. Preparation of the magnetic force application hardware

- 3D print all parts using acrylonitrile butadiene styrene (ABS) and assemble them following the CAD design (Figure 1A). The CAD design is included in the Table of Materials.
- Use double-sided tape to attach the magnet to the magnet-moving device (Figure 1A).
- Set the magnet-moving device next to the microscope stage. Use the three knobs to adjust the spatial location of

the magnet until it can move above the Petri dish between 13 mm and 120 mm.

NOTE: Ensure the upper limit of the distance between the magnet and Petri dish is as large as possible to avoid unwanted force application on the magnetic microbeads. 120 mm is the maximum value in this experimental setup. Ensure that the magnet does not interfere with microscope parts, including objectives and motorized stages.

4. Set the magnet to the highest z-position (at 120 mm).

5. Force application and live-cell imaging

- 1. Set up of the environment chamber for long-term imaging
 - Apply 75% ethanol solution to thoroughly sterilize and clean the environment chamber.
 - Place the environment chamber onto the motorized stage of the inverted microscope.
 - Open the CO₂ tank and set the CO₂ inflow rate to 160 mL/min.
 - Adjust the temperature of the chamber to 44 °C (Top), 42 °C (Bath), and 40 °C (Stage).
 - Add 20 mL of purified water into the bath of the environment chamber to maintain 90% humidity.
 - Take out the glass-bottom Petri dish that contains target cells from the tissue culture incubator and place it into the chamber.
 - Apply the metal clamp of the environment chamber to fix the Petri dish position.

NOTE: The Petri dish must be clamped tightly in the chamber because the magnetic force may move the dish if it is not clamped.

Close the lid of the chamber.



2. Optimization of imaging parameters

- Optimize the pinhole size: The pinhole blocks the out-of-focus photons. A larger pinhole size yields more out-of-focus photons but a brighter image. A smaller pinhole size yields a more focused and dimmer image. Make sure to optimize the pinhole size to get in-focus confocal images with the appropriate signal-to-noise ratio.
- Optimize the laser intensity: The laser intensity
 determines the intensity of excitation and thus
 emission light. The low laser intensity gives a low
 signal-to-noise ratio. Too high a laser intensity will
 cause photobleaching. Adjust the laser intensity
 accordingly.
- 3. Optimize the step size and steps: Steps and step size determine how many images will take in a Z-stack. Smaller step sizes and more steps will increase the Z-stack resolution but will also increase photobleaching. In this experiment, 1 μm step size was used for the cells with ~15 μm cell height.
- 4. Optimize the exposure time: The exposure time determines how long the cell will be exposed to the excitation laser. A low exposure time will decrease the signal-to-noise ratio. A high exposure time will cause photobleaching. An exposure time of 1 frame per 4 s was used in this experiment.
- 5. Optimization of imaging parameters: Change one of the four parameters iteratively and keep the other parameters consistent. Each time, measure the YAP N/C ratio of each image and compare the YAP N/C ratio change to determine the photobleaching level. Repeat the optimization process until achieving a

- balance between the signal-to-noise ratio, imaging speed, and photobleaching.
- Define the imaging configurations using the optimized imaging parameters for faster imaging settings during the experiments.

NOTE: Configurations used in this study are described in section 5.3 of imaging parameters. To optimize imaging parameters of configurations in section 5.3, use the same method as in step 5.2.5.

- Small force application and confocal imaging NOTE: Nikon Ti2-E microscope was used for imaging in this study, and detailed steps for image acquisition are given below.
 - Open the inverted microscope. Open the software application Elements.
 - Define configuration magnetic_find. Check only FITC channel. Set PMT HV = 70, Offset = 0, Laser intensity = 10. Set the scanning speed to 1 frame per 2 s by clicking the 1/2 button. Set pinhole size to 1.2 AU by clicking the 1.2 A.U. button. This configuration will be used in step 5.3.5.
 - 3. Define configuration magnetic_YAP_Nucleus. Check FITC channel. Set PMT HV = 70, Offset = 0, Laser intensity = 10. Set the scanning speed to 1 frame per 4 s by clicking the 1/2 button. Set pinhole size to 1.2 AU by clicking the 1.2 A.U. button. To image the nucleus boundary and nuclear stain intensity, check Cy5 channel. Set PMT HV = 70, Offset = 0, Laser intensity = 10. The pinhole size is optimized for 3D YAP imaging. Do not click the 1.2 A.U. button again after checking the Cy5 channel. This configuration will be used in step 5.3.7.

iove.com



- 4. Turn on **DIA** through **Elements** if necessary. Open **SpinView**, use a bright-field, and adjust the focus of the object to get a clear in-focus image of cells. Use a 10x objective to find appropriate multiple single cells in three conditions: with a single microbead inside, with multiple microbeads inside, and without any microbead inside. Switch to 40x objective. Name this position with the appropriate position number.
- Open Elements. Click on magnetic_find. Click the Remove Interlock button.
- Click Scan and adjust the Z-position of the focal plane. Click the Top and Bottom buttons to set the lower and upper limit for the Z-stack of the selected cells. Stop scanning by clicking Scan again.
- Switch to magnetic_YAP_Nucleus configuration.
 Set file name as before_small_force.nd2. Click on the Run button with the recorded Z-stack.
- 8. Switch to the right light path and turn on DIA. Open SpinView and click on the Recording button. Meanwhile, spin the knob of the magnet-moving device to move the magnet down to 46 mm above the Petri dish bottom. Save bright-field image sequence or video. Check the video to confirm microbeads show displacement induced by magnetic force.
- Repeat steps 5.3.5-5.3.7; set the file name to after_small_force.nd2.
- 10. Switch to the right light path and turn on DIA. Next, open SpinView and click on the Recording button. Meanwhile, spin the knob of the magnet-moving device to move the magnet up to 120 mm above the Petri dish bottom. Save bright-field image sequence or video.

- 11. Repeat steps 5.3.5-5.3.7 and set the file name to **before large force.nd2**.
- 4. Large force application and confocal imaging
 - Remove the lid of the environment chamber to allow the magnet to reach 13 mm above the Petri dish bottom.
 - 2. Switch to the right light path and turn on DIA. Open SpinView and click on the Recording button. Meanwhile, spin the knob of the magnet-moving device to move the magnet down to 13 mm above the Petri dish bottom. Save bright-field image sequence or video. Check the video to confirm microbeads show displacement induced by magnetic force.
 - Repeat steps 5.3.5-5.3.7 and set the file name to after_large_force.nd2.
 - 4. Switch to the right light path and turn on DIA. Next, open SpinView and click on the Recording button. Meanwhile, spin the knob of the magnet-moving device to move the magnet up to 120 mm above the Petri dish bottom. Save bright-field image sequence or video.
 - Repeat steps 5.3.5-5.3.7; set the file name to retract_large_force.nd2.
 - 6. Close the lid of the environment chamber.
- 5. Repeat steps 5.2 and 5.3 for multiple fields of view to obtain more data if needed.

6. Image processing and data analysis

- 1. Quantification of YAP N/C ratio
 - Open Fiji ImageJ. Open the .nd2 images taken in step 5.



- Click on Analyze > Set Measurements. Check Area, Integrated Density, Mean Grey Value, and Shape Descriptors.
- Use the Cy5 channel to identify the nucleus. Click on Freehand Selections to use the free-selection tool to outline the nucleus. Also, check the automatic nuclear mask macro in ImageJ (see the Table of Materials).
- Click Analyze > Measure in the FITC channel. The measured value of the Mean is the average nuclear YAP intensity D_N.
- 5. Use the Cy5 channel to identify the nucleus. Use the FITC channel to identify the cell. Click Freehand Selections to use the free-selection tool to select a region of interest within the cytoplasm and avoid the magnetic microbead. This region of interest must not include the nucleus.
- Click Analyze > Measure in the FITC channel.
 The measured value of the Mean is the average cytoplasmic YAP intensity D_C.
- 7. Calculate the YAP N/C ratio = DN / DC.
- Quantification of nuclear shape and normalized nuclear stain intensity
 - Open Fiji ImageJ. Open the .nd2 images taken in step 5.
 - Click on Analyze > Set Measurements. Check Area, Integrated Density, Mean Grey Value, and Shape Descriptors.
 - Use the Cy5 channel to identify the nucleus. Click on Freehand Selections to use the free-selection tool to outline the nucleus.

- Click on Analyze > Measure in Cy5 channel. The measured value of the Mean is the nuclear stain intensity. The measured value of Circ. is nuclear circularity.
- To compare the nuclear stain intensity at different force state, all nuclear stain intensity is divided by the nuclear stain intensity in "before_small_force.nd2" to generate the normalized nuclear stain intensity.

Representative Results

Design of a magnet-moving device and application of magnetic force

To apply force on the nucleus through the magnetic microbeads, a magnet-moving device was designed and built to control the spatial position of the magnet. The magnet-moving device contains a central frame, three knobs, and rails to move the attached magnet in x, y, and z directions independently at the spatial resolution of 1.59 mm per cycle (**Figure 1A**). Once the magnet is moved close to the 7 µm microbeads delivered into the cells (**Figure 1B**), it magnetically attracts the microbeads and applies force on the nucleus (**Figure 1C**). The force direction and magnitude are controlled by the relative position between the magnet and microbeads.

In this paper, two different magnitudes of force were applied to the microbeads: (1) a relatively small force when the magnet was placed 46 mm above the cell; and (2) a relatively large force when the magnet was placed 13 mm above the cell. The magnetic force applied to the microbead F can be calculated by the equation $F = (1 - N_d)\mu V_p(H \cdot \nabla)H$, where $F = (1 - N_d)\mu V_p(H \cdot \nabla)H$, where $F = (1 - N_d)\mu V_p(H \cdot \nabla)H$, where $F = (1 - N_d)\mu V_p(H \cdot \nabla)H$ is the permeability in a vacuum (6.3 × 10⁻³ H/m for iron), $F = (1 - N_d)\mu V_p(H \cdot \nabla)H$ is the volume of the microbead (178 μ m) for a 7 μ m microbead), and $F = (1 - N_d)\mu V_p(H \cdot \nabla)H$ is the



magnetic field intensity with the unit A/m. H is proportional to magnetic flux density **B** with unit Tesla. Since the magnetic force acting on a single 7 µm microbead was expected to be extremely small and difficult to detect by a force transducer, the magnetic flux density **B** as a reference was measured to indicate the magnitude of the magnetic force applied on the microbeads. A Hall sensor was introduced at the location of the Petri dish bottom to measure the magnetic flux density, and the magnet was placed at a distance of 13 mm or 46 mm from the bottom of the Petri dish. Because the 7 um microbeads influence the magnetic field, the magnetic flux density was measured with and without microbeads. Regardless of the presence of the 7 µm microbeads, the same magnetic flux density was obtained: $B = 60.1 \, mT$ at a distance of 13 mm and B = 3.7 mT at a distance of 46 mm. This measurement shows that the effect of 7 µm microbeads on the magnetic field generated by the cylindrical magnet with 12.7 mm diameter and 12.7 mm height (see the Table of Materials) was not detectable by the Hall sensor used in this study. However, the magnetic flux density in the case with a 13 mm distance was about 16 times higher than that with a 46 mm distance. Experimental calibration of the magnetic force is described in the following section (Figure 6).

Delivery of magnetic microbeads into the cytoplasm

12 h after seeding cells on the glass-bottom Petri dish, 7 μm microbeads are added into the culture medium. Microbeads are spontaneously internalized by the cells. Because the microbeads do not emit fluorescence under laser excitation in FITC or Cy5 channel, the location of the internalized microbeads can be identified by the location of the dark hollow with the confocal imaging of fluorescence of YAP and nucleus. Both 2D and 3D images show that the microbead is in the cytoplasm while outside the nucleus (**Figure 2**).

The internalization levels of microbeads into the cells depend on the duration of the co-culture of cells and microbeads. Thus, the cells were categorized into three types according to the quantity of internalized microbeads-no microbead, single microbead, and multi-microbeads (**Figure 3A**). At 7 h of co-culture, 62% of the cells internalized no microbead, 15% of the cells internalized a single microbead, and 23% of the cells internalized multi-microbeads (total number of cells = 13). At 12 h of co-culture, 53% of the cells internalized no microbead, 26% of the cells internalized a single microbead, and 21% of the cells internalized multi-microbeads (total number of cells = 62). At 24 h of co-culture, 20% of the cells internalized no microbead, 28% of the cells internalized a single microbead, and 53% of the cells internalized multi-microbeads (total number of cells = 40) (**Figure 3B**).

Microbeads in cytoplasm do not influence nuclear shape and YAP activity

To examine the effect of the internalization of microbeads on nuclear shape and protein activity, the nuclear shape was firstly quantified by circularity and the YAP activity by YAP N/ C ratio, respectively. Circularity is calculated by Circularity = 4u (area / perimeter²). The detailed steps to quantify YAP N/C ratio were described in a previous publication 60. Briefly, YAP N/C ratio was calculated by dividing the mean YAP intensity in the nucleus by the mean YAP intensity in the cytoplasm. Considering the possibility that co-culture of microbeads and cells can influence the nuclear shape even if no microbead is internalized, the cells without co-culture (black dots, control #1, Circularity = 0.806 ± 0.037 , n = 20), cells co-cultured with microbeads but without internalization (grey dots, control #2, Circularity = 0.806 ± 0.035 , n = 22), cells internalizing single microbead (red dots, single microbead, Circularity = 0.793 ± 0.048, n = 15), and cells internalizing multi-microbeads (blue dots, multi-microbeads, n = 7) (Figure 3C) were compared.



The result shows that among all four groups tested, nuclear circularity had no significant difference (**Figure 3C**).

Next, to examine whether YAP N/C ratio is influenced by the internalization of microbeads, the cells co-cultured with microbeads but without internalization (grey dots, control #2, YAP N/C ratio = 1.155 ± 0.074 , n = 35) were compared only with the cells with single or multi-microbead internalization (red dots, cell with microbeads, YAP N/C ratio = 1.140 ± 0.078 , n = 36) at the 12^{th} hour of co-culture (**Figure 3D**). The cells without co-culture were not compared because the dish with microbeads shows lower cell density, which may influence the YAP N/C ratio 12 . The result shows no significant difference (p value = 0.667) in the YAP N/C ratio between the two groups, indicating that the internalization of microbeads does not influence the YAP activity (**Figure 3D**).

Magnetic force deforms the nucleus

First, the deformation of the nucleus is shown. The deformation of the nucleus is caused by the compression force applied by the microbeads (Figure 4A and Figure 4A1-3) in cells that contain cytoskeleton. This data (i.e., the nucleus being deformed by the microbead's compression) supports that the microbead is indeed applying a force onto the nucleus in the crowded cytoplasm. A bright-field video showing the force application process is included in the supplement material (Supplementary Video 1). Second, because it is possible that the microbead simultaneously applies force on the surrounding cytoskeleton and deforms the nucleus indirectly, the compression experiments were repeated in cells that have the disrupted actin filaments (treatment of Cyto D (2.5 µM, 1 h); Figure 4B). This study shows that the actin filaments are indeed depolymerized (Figure 4B), and the nucleus is deformed by the microbeads (Figure 4B1-3). This data supports that the microbeads are applying a force directly onto the nucleus in the absence of intertwined surrounding cytoskeleton. Collectively, this data shows that the protocols and tools can apply a force directly onto the nucleus.

Spatial and temporal control of intracellular magnetic microbeads

To achieve spatial control of the microbeads, a pair of magnets were used to move the microbead and control its location of the indentation onto the nucleus (**Figure 5A**). The bead can only be moved with up to 2.2 μ m of displacement (**Figure 5A1-4**), but can flexibly apply indentation on the nucleus at corresponding locations. The surrounding actin cytoskeleton may restrict the movement of microbeads. Therefore, the actin cytoskeleton was disrupted by Cyto D treatment (2.5 μ M, 1 h), and the microbead location was manipulated but showed similar results. Therefore, a hypothesis can be proposed: the microbead may physically/ chemically bind with the nucleus and other surrounding organelles in the cytoplasm, which restricts its large spatial movement (>2.2 μ m).

To achieve spatial control of the microbeads, a pair of magnets was used that controls the microbeads to apply and release the force twice (with different force magnitude) at the same location of the nucleus (**Figure 5B** and **Figure 5B1-B4**). The current time duration for one cycle of force application and releasing is 12 s. The speed of temporal control is determined by the operation speed of the XYZ mover.

Calibration of the magnetic force

The bead-applied force onto the nucleus was estimated by experimentally measuring the force applied by a calibrated atomic force microscopy (AFM) that causes a similar deformation of the nucleus. Specifically, the actin



cytoskeleton was first dissolved by CytoD (2.5 µM; 1 h, Figure 4B) because the AFM applies force on the cell's apical surface, and the removal of actin cortex and cytoskeleton allows more direct contact between AFM tip and cell nucleus. The cells that have their actin cortex and cytoskeleton dissolved are alive based on the comparison of nuclear shape and nuclear staining intensity with those in healthy cells (Supplementary Figure 1). Second, the un-functionalized AFM tip (semi-spherical, radius = 5 µm) that has a similar size and shape as those of the microbeads was used to indent the cell's apical surface in a force-controlled manner and simultaneously acquire 3D confocal images of the cell and nucleus bodies (Figure 6A). The magnitude of the compressive force from 0.8 nN to 2.0 nN was chosen because, based on the literature²⁴, force at a magnitude of 1.5 nN was known to sufficiently deform the nucleus. Third, the normal deformation of the nucleus that was caused by the AFM indentation was measured through quantitative imaging analysis. Also, the calibration curve that provides the quantitative AFM force-displacement relationship (Figure 6B) was obtained. Fourth, a compressive force was applied to the lateral surface of the nucleus by controlling micro-beads that have similar size and shape (radius = 7 µm; Figure 6C), and the deformation of the nuclear membrane was measured via imaging analysis. The beads-applied force is estimated based on the AFM force-displacement relationship.

For example, in **Figure 6C**, the deformation of the nucleus caused by magnetic microbeads (diameter = \sim 7 µm) at 'large force' is around 1.5 µm. In **Figure 6D**, an AFM tip that has a 5 µm semispherical probe was used to indent the cell on top of the nucleus to achieve 1.5 µm nuclear deformation. The corresponding force recorded by AFM is 1.4 nN. Hence, the force applied by the microbeads is estimated to be \sim 1.4 nN. Following the same approach, the magnetic force at 'small

force' is calibrated as 0.8 nN, and it caused 0.4 μm nuclear indentation.

This study considers that the AFM-measured force can represent the microbead-applied force based on the following assumptions: (1) The stiffness of the nucleus within different cells is similar. (2) The mechanical properties of the nucleus are not dependent on the nuclear sites on which the indentation was applied. The magnetic force is applied horizontally on the lateral sides of the nucleus, while the AFM force is applied vertically on the apical sides of the nucleus. The mechanical difference between them is assumed as negligible. (3) In AFM experiments, the probe is directly applying force through the cell membrane and cytoskeleton onto the nucleus. After disrupting the actin filaments, the AFM-applied force onto the nucleus is similar to the microbeads-applied force onto the nucleus, despite the membrane still located between the AFM probe and the nucleus in the former case.

Magnetic force triggers change of YAP N/C ratio

To prove that the magnetic force applied on the microbeads can deform the nucleus and induce YAP translocation, the YAP N/C ratio of the cells with microbeads internalization was quantified in three stages: (1) before applying the force, (2) after applying the force, and (3) after releasing the force. Some cells showed a change of nuclear shape and YAP N/C ratio when the force was applied or released (**Figure 7A,C**). The intensity changes in YAP can be attributed by two possible mechanisms: (1) YAP-FP proteins translocate from the cytoplasm into the nucleus after force application. In this case, nuclear staining should show no signal changes. Nuclear staining intensity should not change largely; (2) YAP-FP proteins do not translocate after force application. The observed YAP intensity changes are due to the force-



induced nuclear volume change and the resulting YAP-FP concentration change. In this case, the nuclear staining intensity should change in a similar trend as the YAP nuclear intensity because the concentration of staining dye also changes as the nucleus volume alters. Therefore, the nuclear staining intensity change from the red channel (excitation: 650 nm; emission: 681 nm) was measured. The intensity changes in YAP in the green channel, but there are no intensity changes in nucleus staining in the red channel. Thus, the first mechanism likely exists (**Figure 7B**). Collectively, the results show that the magnetic force-induced nuclear deformation triggers YAP translocation.

Next, the net change of YAP N/C ratio was quantified within two groups of cells: (1) cells without microbead internalized (grey dots, control, n = 9); and (2) selected cells with internalized microbead(s) that show change of YAP N/C ratio (green dots for small force, red dots for large force, n = 11).

At 0.8 nN force, cells with internalized microbead(s) show net YAP N/C ratio change = -0.030 ± 0.029 , n = 11; control cells show net YAP N/C ratio change = -0.003 ± 0.012 , n = 9. At 1.4 nN force, cells with internalized microbead(s) show net YAP N/C ratio change = 0.011 ± 0.040 , n = 11; control cells show net YAP N/C ratio change = 0.005 ± 0.005 , n = 9 (Figure 8A). At 0.8 nN force, cells with internalized microbead(s) show absolute net YAP N/C ratio change = 0.057 ± 0.017 , n = 11; control cells show net YAP N/C ratio change = 0.021 ± 0.007 . n = 9. The difference is significant (p value = 0.0093, **). At 1.4 nN force, cells with internalized microbead(s) show absolute net YAP N/C ratio change = 0.070 ± 0.020 , n = 11; control cells show net YAP N/C ratio change = 0.010 ± 0.003 , n = 9. The difference is significant (p value = 0.0007, ***) (Figure 8B). Together, these results corroborate that the magnetic force applied to the microbeads within the cytoplasm can indeed induce YAP translocation and change YAP N/C ratio.



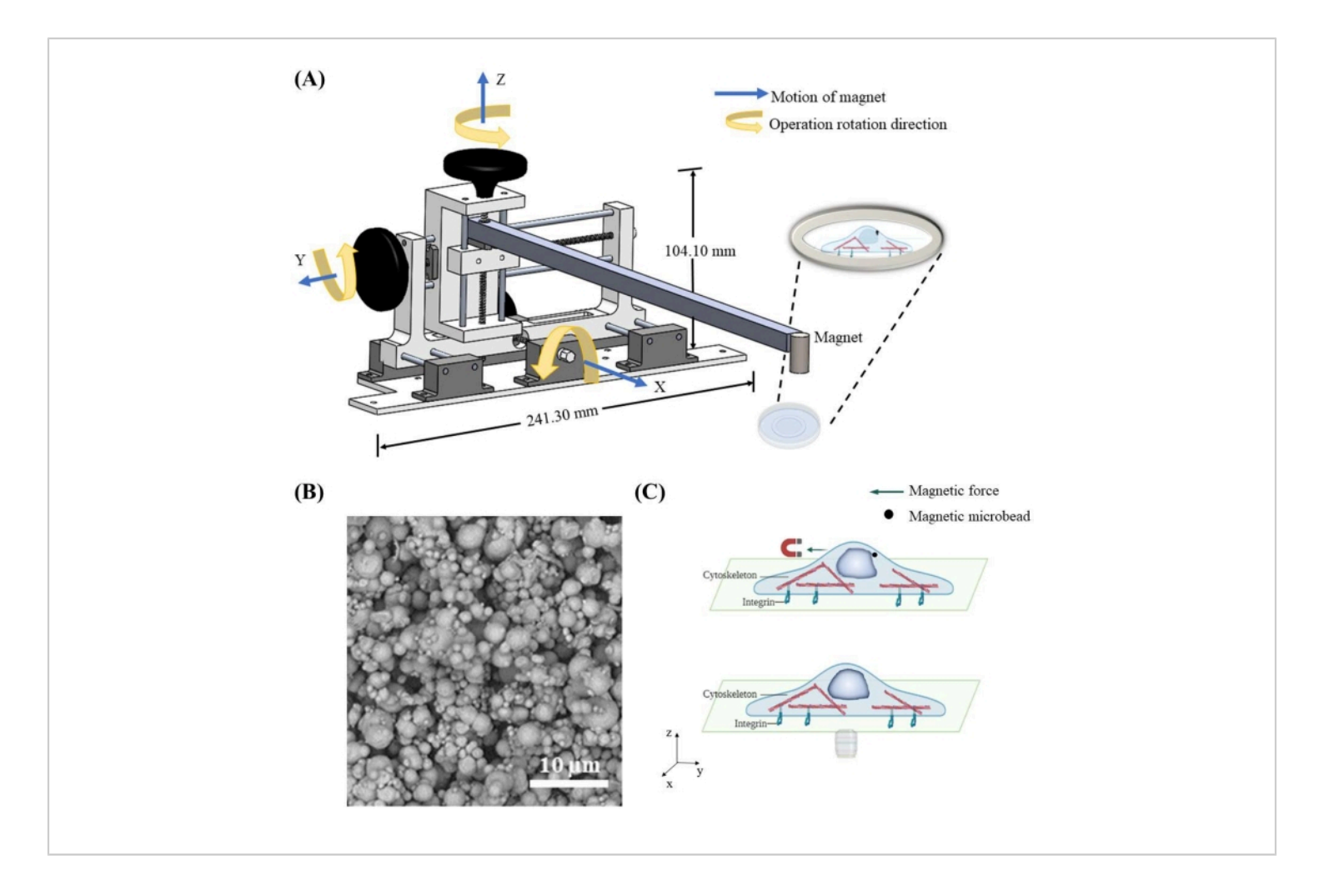


Figure 1: Design of the magnetic moving device and schematic force application in the cell by magnetic

microbeads. (A) Three-dimensional schematic of the device implemented to hold the magnet and move it in x, y, and z directions. The device consists of a base 241.3 mm in width and 104.1 mm in height, two knobs, a bar, and a magnet. The knobs will be splined in the correct operation rotation direction, which will deliver movement in the corresponding direction. The magnet will be lowered closer/raised further to the dish to apply magnetic force with different magnitude and direction on magnetic microbeads. (B) Example scanning electron microscope (SEM) image of 7 μm iron microbead. (C) Magnetic microbeads delivered inside the cytoplasm can apply force to the organelles such as the nucleus when a magnetic field is applied. Please click here to view a larger version of this figure.



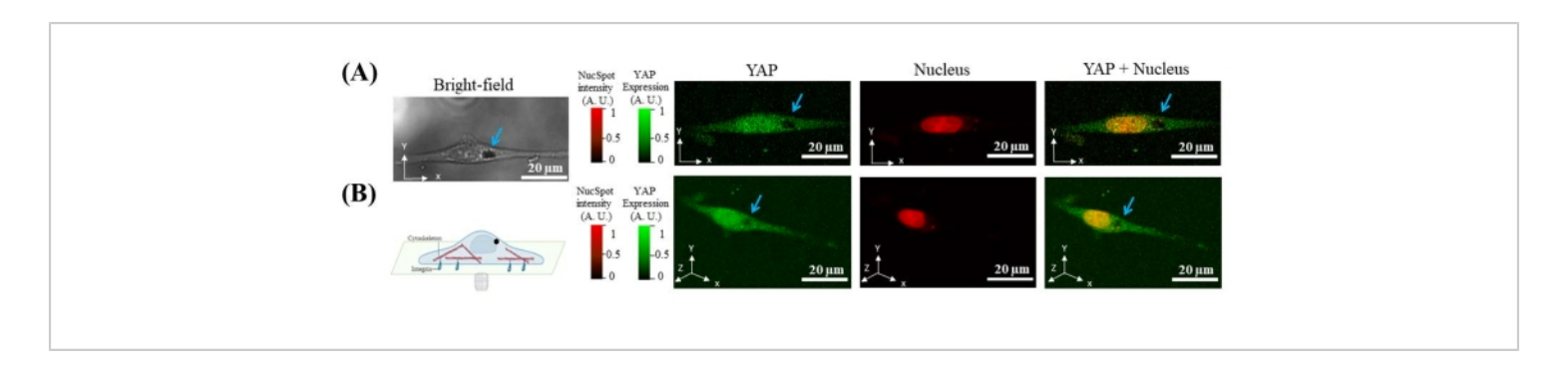


Figure 2: Representative images showing magnetic microbead (black hollow pointed by blue arrow) is internalized into the cell (indicated by YAP) and outside the nucleus. (A) X-Y cross-section of a cell of YAP (green), nucleus (red), and bright-field. (B) 3D reconstruction of the cell. Please click here to view a larger version of this figure.



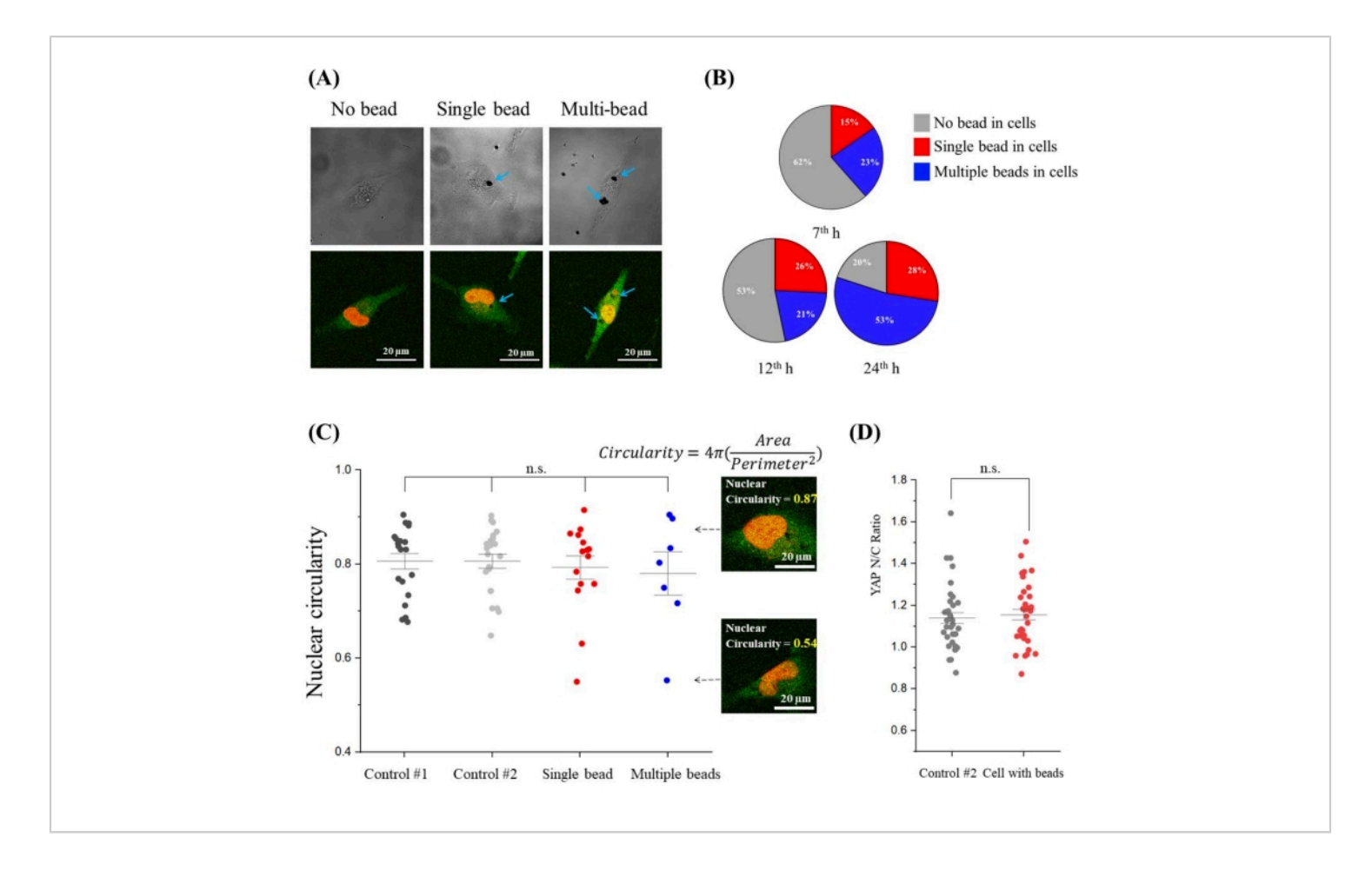


Figure 3: Microbeads internalized by the cells do not affect the nuclear shape and YAP N/C ratio. (A) Representative bright-field and fluorescence images of cells with no microbead, single microbead, and multi-microbead internalization.

Blue arrows indicate the position of microbeads inside the cytoplasm. (B) At 7 h (n = 13), 12 h (n = 62), and 24 h (n = 40) of co-culture, the percentage of the cells showing no microbead, single microbead, and multi-microbead internalization. (C) Nuclear circularity shows no significant difference between control cells and cells with microbead internalization. Control #1 (without microbead co-culture): Circularity = 0.806 ± 0.037 , n = 20; Control #2 (with microbead co-culture, without microbead internalization): Circularity = 0.806 ± 0.035 , n = 22; Single microbead internalization: Circularity = 0.793 ± 0.048 , n = 15; multi-microbead internalization: Circularity = 0.780 ± 0.061 , n = 7. (D) YAP N/C ratio show no significant difference (p value = 0.667) between control cells (with microbead co-culture, without microbead internalization, YAP N/C ratio = 1.155 ± 0.074 , n = 35) and cells with microbead internalization (YAP N/C ratio = 1.140 ± 0.078 , n = 36). Please click here to view a larger version of this figure.

iove.com



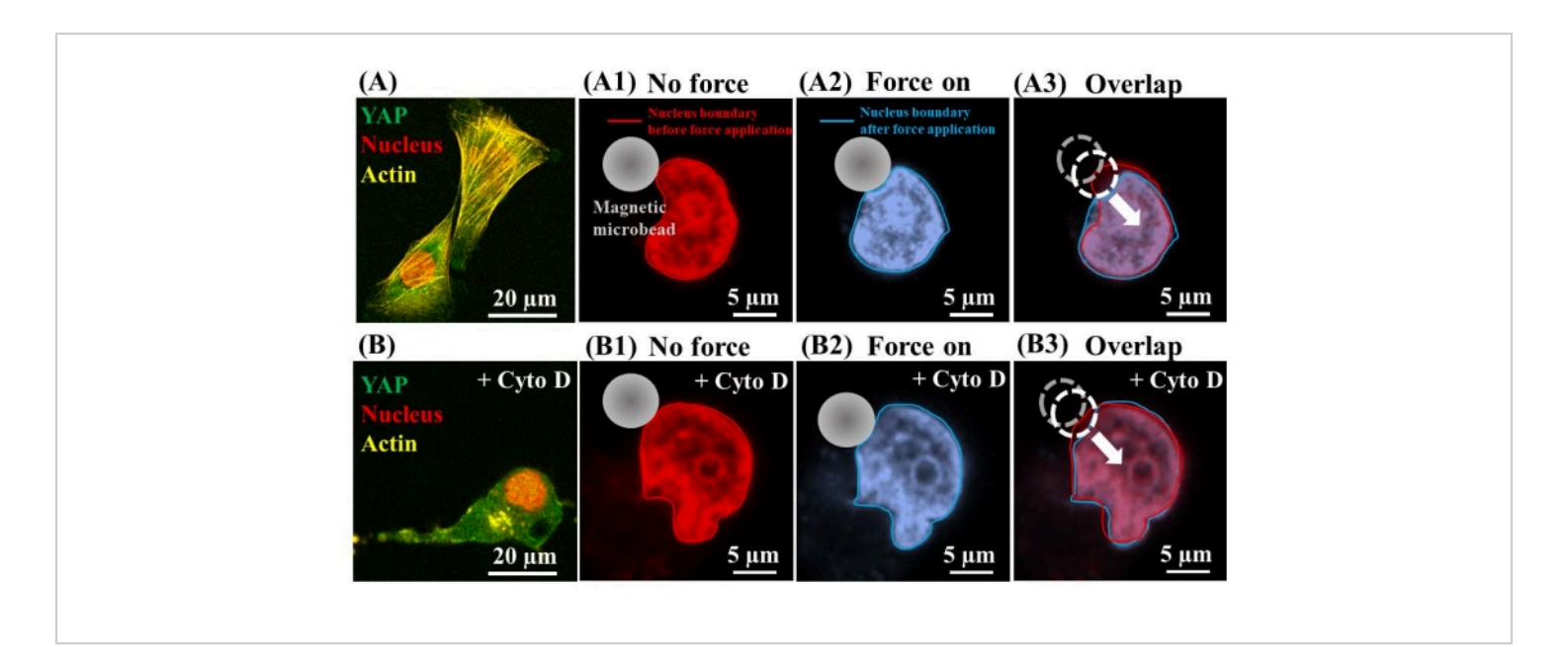


Figure 4: Direct force application on nucleus with and without actin filaments. (A) Cells show actin filaments (yellow). (A1) Image of the nucleus when no force is applied. (A2) Image of the nucleus after the force is applied. (A3) Overlap image of the nuclear boundary before and after the force application shows nuclear indentation. (B) Cells show disrupted actin filaments (yellow) after Cyto D treatment (2.5 μM, 1 h). (B1) Image of the nucleus when no force is applied. (B2) Image of the nucleus after the force is applied. (B3) Overlap image of the nuclear boundary before and after the force application shows nuclear indentation with the disrupted actin cytoskeleton. Please click here to view a larger version of this figure.



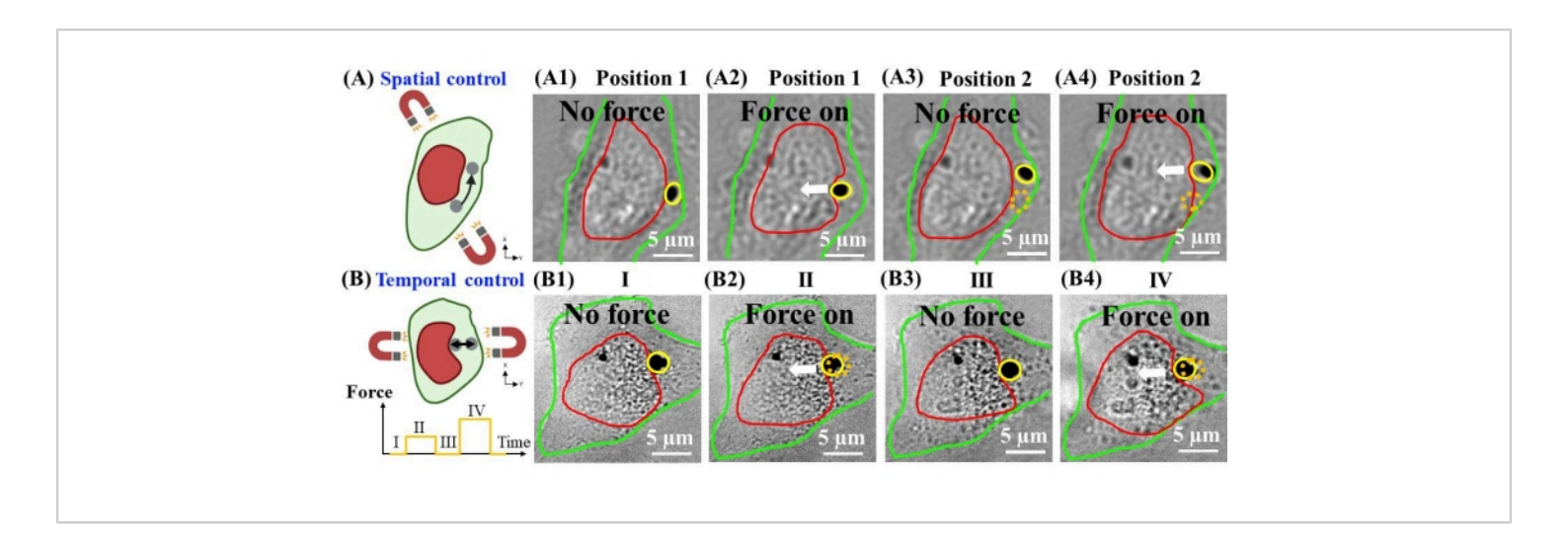


Figure 5: Spatial and temporal control of intracellular magnetic microbead. (A) A pair of magnets spatially controls the magnetic microbead. (A1) Bright-field image of cell boundary (green line), nuclear boundary (red line), and magnetic microbead (yellow line) at position 1. (A2) Magnetic microbead indents nucleus at position 1. (A3) Magnetic microbead is moved to position 2 (yellow line). Position 1 is shown as a reference (yellow dashed line). (A4) Magnetic microbead indents nucleus at position 2. (B) A pair of magnets temporally controls magnetic microbead. (B1) Bright-field image of a cell with no force applied at time point I. (B2) Magnetic microbead applies a force onto the nucleus at time point II. (B3) Magnetic microbead releases the force from the nucleus at time point III. (B4) Magnetic microbead applies a larger force onto the nucleus at time point IV. Please click here to view a larger version of this figure.



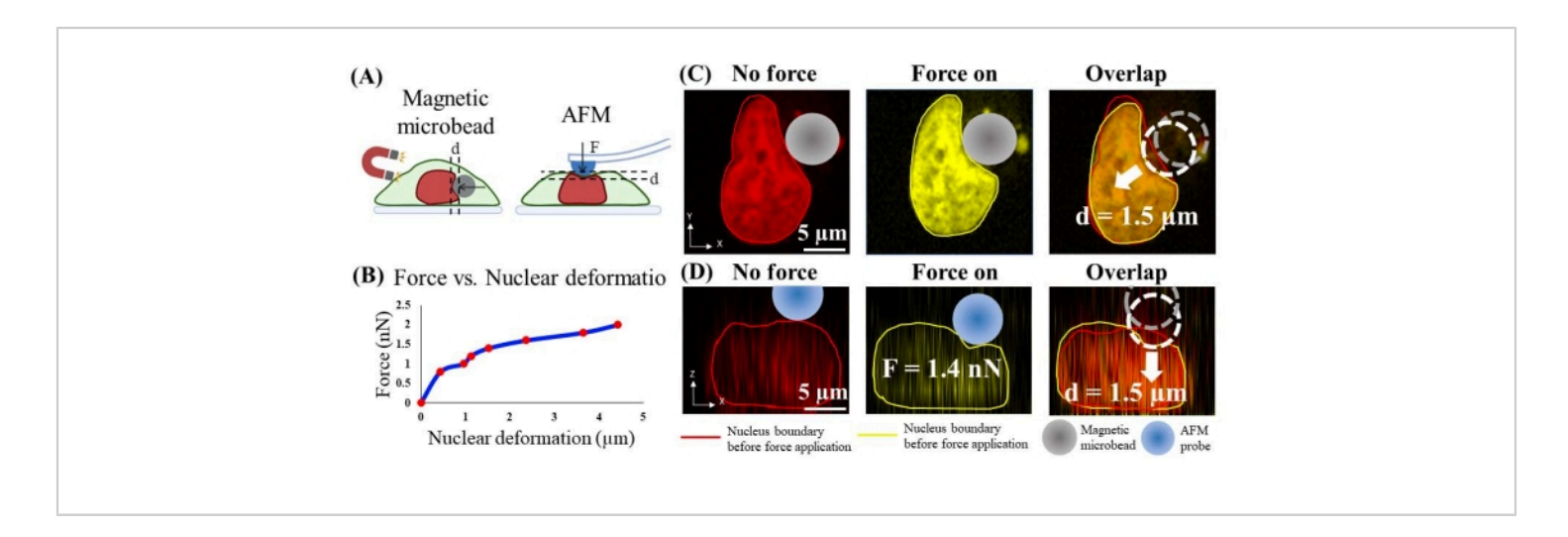


Figure 6. Calibration of microbead-applied force on the nucleus using AFM indentation. (A) Schematic illustration of the calibration process. Magnetic microbead applies horizontal compression on the nucleus (left), and AFM probe indents vertically on the nucleus. (B) AFM indentation force vs. nuclear deformation. (C) Representative image of nucleus deformation (1.5 μm) before and after force application by magnetic microbead. (D) Representative image of similar nucleus deformation (1.5 μm) before and after AFM indentation with 1.4 nN force. Please click here to view a larger version of this figure.



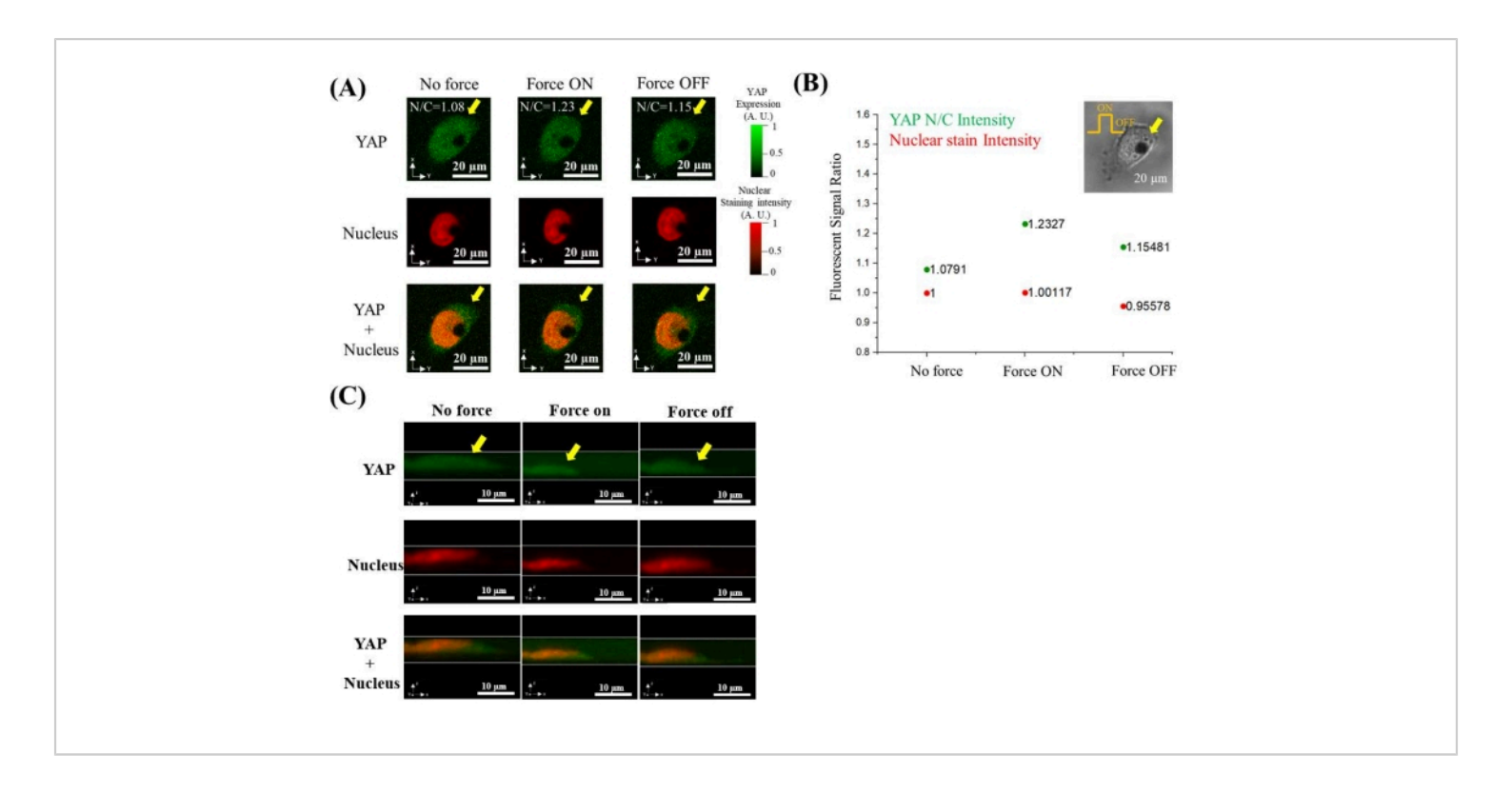


Figure 7: Representative data showing YAP N/C ratio change is induced by magnetic force application and release.

(A) X-Y cross-section of YAP (green) and nucleus (red) fluorescent image of the cell at no force, force on, and force off. In the force-on condition, cytoplasmic YAP intensity decreases at the location pointed by a yellow arrow while nuclear YAP intensity increases. YAP N/C ratio increases. (B) YAP N/C ratio increases when force on (from 1.0791 to 1.2327) and decreases when force off (from 1.2327 to 1.1548). Normalized nuclear stain intensity shows minor change with force application (1.00117) and releasing (0.95578). (C) X-Z cross-section of YAP (green) and nucleus (red) image of the cell at no force, force on, and force off. Please click here to view a larger version of this figure.



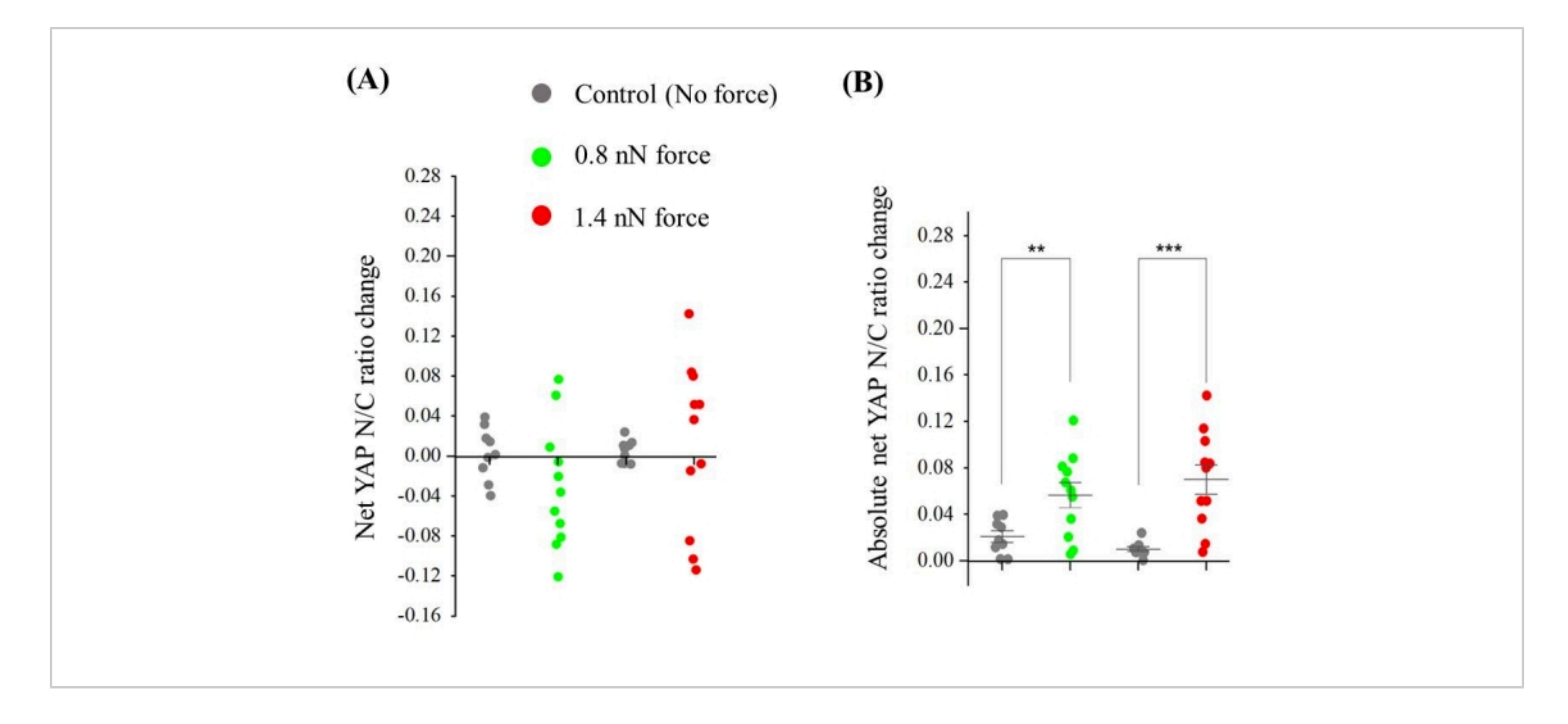


Figure 8: YAP N/C ratio change induced by magnetic force application. (A) At 0.8 nN force, cells with internalized microbead(s) show net YAP N/C ratio change = -0.030 ± 0.029 , n = 11; control cells show net YAP N/C ratio change = -0.003 ± 0.012 , n = 9. At 1.4 nN force, cells with internalized microbead(s) show net YAP N/C ratio change = 0.011 ± 0.040 , n = 11; control cells show net YAP N/C ratio change = 0.005 ± 0.005 , n = 9. (B) At 0.8 nN force, cells with internalized microbead(s) show absolute net YAP N/C ratio change = 0.057 ± 0.017 , n = 11; control cells show net YAP N/C ratio change = 0.021 ± 0.007 , n = 9. The difference is significant (p value = 0.0093, **). At 1.4 nN force, cells with internalized microbead(s) show absolute net YAP N/C ratio change = 0.070 ± 0.020 , n = 11; control cells show net YAP N/C ratio change = 0.010 ± 0.003 , n = 9. The difference is significant (p value = 0.0007, ***) Please click here to view a larger version of this figure.

Supplementary Figure 1: Nuclear shape and nuclear staining intensity. (A) Without Cyto D treatment, (B) With Cyto D treatment and (C) Dead cell. Please click here to download this File.

Supplementary Video 1: A bright-field video showing the force application process. Please click here to download this Video.

Discussion

Internalization of magnetic microbeads (section 2.2) is critical because extracellular microbeads cannot apply force directly

to the nucleus. Force application and imaging (section 5.3) are critical steps in this experiment, and the force needed to deform the nucleus and induce meaningful biological consequences might be sample-dependent. The force magnitude in this experiment (0.8 nN and 1.4 nN) can be further increased to trigger nuclear mechano-sensing in less sensitive cells.

To apply magnetic force in a quantitative manner with high throughput, the internalization of a single microbead is an ideal approach. In this study, the percentage of the cells with single-microbead internalization was similar at 12 h



(26%) and 24 h (28%), while the cells without microbead internalization were higher at 12 h (53%) than that at 24 h (20%) (**Figure 3B**). It is considered that 12 h is the optimal time for force-application experiment because more single microbeads can be included, and cells can be controlled. For different cell lines and microbead sizes, co-culture time and microbead concentration should be tested to determine the corresponding optimal conditions.

In the experiments, the microbeads were not coated to specifically bind to the nucleus. Therefore, the force directly transmitted from the microbeads to the nucleus is likely only compressive. The results show that the YAP N/C ratio increases and decreases the cell population (**Figure 8A**). One possible reason is that the magnetic force applied *via* the microbeads may cause positive or negative tension change within the cytoskeleton and regulate YAP N/C ratio to increase or decrease, respectively²⁸. Previous research shows that compressive force on the nucleus induces an increase in the YAP N/C ratio²⁸. In future experiments, in order to study the direct force sensing of the nucleus, the cytoskeleton can be disrupted to eliminate the force transmission from the cytoskeleton into the nucleus.

There are two potential drawbacks in the current methods. First, in these experiments, the 3D mover (**Figure 1A**) was utilized to adjust the beads' motion, which is monitored by real-time confocal imaging and aims to apply a compressive force on the nucleus. However, due to the slippery nature of the nuclear membrane and the complex environment in the cytoplasm, the direction of the beads-applied force may not be purely compressive (i.e., not absolutely perpendicular to the nuclear membrane surface). This imperfection can cause a shear force to be applied to the nuclear membrane. Second, the current microbeads used in this study are not conjugated

with the antibody to bind with the nucleus, because the spatial mobility of the beads is critical in the current experiment to demonstrate the advantage of non-contact magnetic actuator. Hence, the current method cannot apply tension to the nuclear membrane.

In the future, (1) beads with anti-nesprin-1 antibody will be conjugated to specifically bind with the nucleus. This can quarantee the direct and specific force transmission between microbeads and the target proteins. (2) The direction of force will be calibrated by manipulating the single magnetic microbead in soft hydrogel embedded with fluorescent beads. The 3D displacement of fluorescent beads can be used to calculate the deformation field of the hydrogel and determine the force direction as a function of the applied magnetic field. After the microbead is chemically bonded with the nucleus, applying a force with a known direction will determine the force type (tension, compression, or shear). (3) The 3D imaging of nuclear staining will be used to build a 3D simulation FEM model of the nucleus. The force direction can be verified by comparing the nuclear deformation before and after the magnetic force application.

The unique technique developed in this study provides several potential advantages: (1) Compared to vertical indentation by AFM probes, magnetic microbeads can apply force in any direction. Cells cultured on 2D substrate surfaces may have heterogeneous protein distribution and orientation on their vertical and horizontal surfaces of the plasma membrane and nuclear envelope. Applying force horizontally may induce previously unobserved mechanosensing responses. (2) Once the microbeads are functionally coated to bind to the nuclei, both pushing and pulling forces can be applied directly on the nucleus to further study the differential nuclear mechano-sensing due to the distinct



force directions. (3) By controlling the specific binding of microbeads to certain nuclear envelope proteins, previously under-investigated mechanisms of nuclear force sensing can be elucidated. Emerging evidence shows that the nucleus is likely a mechano-sensor³⁶, and nuclear mechanosensing is the most direct regulator of YAP translocation²⁸. The mechanism of nuclear regulated YAP translocation is actively studied and several candidates of mechanosensor or parameters in the nucleus are proposed, including nuclear pore size 28 , nuclear shape 25,61 , LINC complex. and nuclear envelope tension²⁰. Manipulating the magnetic microbeads opens the possibility for detailed exploration of such mechanisms by direct force application on the LINC complex and controlled regulations of the nuclear-envelope tension and shape. (4) In addition to applying forces on the nucleus, microbeads are also suitable to be engineered to bind to the inner side of the plasma membrane to reveal how the intracellular domains of membrane proteins and their complex respond to biophysical signals.

In summary, this paper demonstrated a method that (1) delivers micro-size iron microbeads into cytoplasm without affecting nuclear morphology and protein functions, (2) applies force on the nucleus by magnetic microbeads, and (3) performs confocal fluorescence live-cell imaging during the force application. These non-invasive tools open the possibilities for direct epigenetic manipulation of organelles in single cells, super-resolution-imaging-based interrogation of nucleus mechanotransduction, and detailed exploration of force-regulated 3D chromosome organization (in combination with Hi-C: high-resolution chromosome confirmation capture) and reprogramming in the contexts of cell physiology and pathobiology.

Disclosures

There are no conflicts of interest to declare.

Acknowledgments

This project is funded by UF Gatorade Award Start-up Package (X. T.), the UFHCC Pilot Award (X. T. and Dr. Dietmar Siemann), UF Opportunity Seed Fund (X. T.), and UFHCC University Scholars Program (H. Y. Wang). We sincerely appreciate the intellectual discussions with and the technical support from Dr. Jonathan Licht (UFHCC), Dr. Rolf Renne (UFHCC), Dr. Christopher Vulpe (UFHCC), Dr. Blanka Sharma (BME), Dr. Mark Sheplak (MAE & ECE), Dr. Daniel Ferris (BME), Dr. Malisa Sarntinoranont (MAE), Dr. Ashok Kumar (MAE), Dr. Benjamin Keselowsky (BME), Dr. Brent Gila (RSC), Dr. Philip Feng (ECE), Dr. Gregory A. Hudalla (BME), Dr. Steven Ghivizzani (OSSM), Dr. Yenisel Cruz-Almeida (CDBS), Dr. Roger Fillingim (CD-BS), Dr. Robert Caudle (OMS), Dr. John Neubert (DN-OR), Dr. Justin Hiliard (Neurosurgery), Dr. Tian He (Harvard University), Dr. Youhua Tan (Hong Kong Polytechnic University), Dr. Jessie L-S Au (Institute of Quantitative Systems Pharmacology), Dr. David Hahn (University of Arizona), and Support Team of Nikon (Drs. Jose Serrano-Velez, Larry Kordon, and Jon Ekman). We are deeply grateful for the effective support from all members of Tang's, Yamaguchi's, Sharma's, Au's, Siemann's, and Guan's research laboratories and all staff members of the UF MAE Department.

References

 Discher, D. E., Janmey, P., Wang, Y. Tissue cells feel and respond to the stiffness of their substrate. *Science*. 310 (5751), 1139-1143 (2005).



- Janmey, P. A., Fletcher, D. A., Reinhart-King, C. A. Stiffness sensing by cells. *Physiological Reviews*. 100 (2), 695-724 (2020).
- Bajaj, P., Tang, X., Saif, T. A., Bashir, R. Stiffness of the substrate influences the phenotype of embryonic chicken cardiac myocytes. *Journal of Biomedical Materials Research Part A.* 95 (4), 1261-1269 (2020).
- Tang, X. et al. Mechanical force affects expression of an in vitro metastasis-like phenotype in HCT-8 cells. Biophysical Journal. 99 (8), 2460-2469 (2010).
- Hofmann, M. et al. Lowering of tumor interstitial fluid pressure reduces tumor cell proliferation in a xenograft tumor model. *Neoplasia*. 8 (2), 89-95 (2006).
- Yankaskas, C. L. et al. The fluid shear stress sensor TRPM7 regulates tumor cell intravasation. Science Advances. 7 (28), eabh3457 (2021).
- Kim, E. et al. A biosynthetic hybrid spidroin-amyloidmussel foot protein for underwater adhesion on diverse surfaces. ACS Applied Materials and Interfaces. 13 (41), 48457-48468 (2021).
- Tajik, A. et al. Transcription upregulation via force-induced direct stretching of chromatin. *Nature Materials*.
 15 (12), 1287-1296 (2016).
- Lee, J., Abdeen, A. A., Tang, X., Saif, T. A., Kilian, K.
 A. Matrix directed adipogenesis and neurogenesis of mesenchymal stem cells derived from adipose tissue and bone marrow. *Acta Biomaterialia*. 42, 46-55 (2016).
- Lee, J., Abdeen, A. A., Tang, X., Saif, T. A., Kilian, K. A. Geometric guidance of integrin mediated traction stress during stem cell differentiation. *Biomaterials*. 69, 174-183 (2015).

- Ren, B. et al. Study of sacrificial ink-assisted embedded printing for 3D perfusable channel creation for biomedical applications. *Applied Physics Reviews*. 9 (1), 011408 (2022).
- Coyle, S. et al. Cell alignment modulated by surface nano-topography-Roles of cell-matrix and cell-cell interactions. Acta Biomaterialia. 142, 149-159 (2022).
- Sawada, Y. et al. Force sensing by mechanical extension of the Src family kinase substrate p130Cas. *Cell.* 127 (5), 1015-1026 (2006).
- Aragona, M. et al. A mechanical checkpoint controls multicellular growth through YAP/TAZ regulation by actin-processing factors. *Cell.* 154 (5), 1047-1059 (2013).
- Tang, X. et al. Specific and non-specific adhesion in cancer cells with various metastatic potentials. *Mechanobiology of Cell-Cell and Cell-Matrix Interactions*. 105-122, Springer, Boston, MA, (2011).
- Tang, X., Saif, T. A. Adhesivity of colon cancer cells during in vitro metastasis. *International Journal of Applied Mechanics*. 5 (03), 1350025 (2013).
- 17. Chaudhuri, O. et al. Effects of extracellular matrix viscoelasticity on cellular behaviour. *Nature*. **584** (7822), 535-546 (2020).
- Ohashi, K., Fujiwara, S., Mizuno, K. Roles of the cytoskeleton, cell adhesion and rho signalling in mechanosensing and mechanotransduction. *The Journal of Biochemistry.* 161 (3), 245-254 (2017).
- Hamill, O. P., Martinac, B. Molecular basis of mechanotransduction in living cells. *Physiological Reviews*. 81 (2), 685-740 (2001).



- Liang, C. et al. Towards an integrative understanding of cancer mechanobiology: Calcium, YAP, and microRNA under biophysical Forces. *Soft Matter.* 18, .1112-1148 (2022).
- Tan, Y. et al. Matrix softness regulates plasticity of tumour-repopulating cells via H3K9 demethylation and Sox2 expression. *Nature Communications*. 5 (1), 1-12 (2014).
- 22. Poh, Y. et al. Dynamic force-induced direct dissociation of protein complexes in a nuclear body in living cells.

 Nature Communications. 3 (1), 1-10 (2012).
- Tang, X. et al. A mechanically-induced colon cancer cell population shows increased metastatic potential. *Molecular Cancer.* 13 (1), 1-15 (2014).
- 24. Wu, J. et al. Effects of dynein on microtubule mechanics and centrosome positioning. *Molecular Biology of the Cell.* **22** (24), 4834-4841 (2011).
- Tang, X., Ali, M. Y., Saif, M. T. A novel technique for micro-patterning proteins and cells on polyacrylamide gels. Soft Matter. 8 (27), 7197-7206 (2011).
- Tang, X., Bajaj, P., Bashir, R., Saif, T. A. How far cardiac cells can see each other mechanically. *Soft Matter.* 7 (13), 6151-6158 (2011).
- Tang, X. et al. Mechanical force affects expression of an in vitro metastasis-like phenotype in HCT-8 cells. Biophysical Journal. 99 (8), 2460-2469 (2010).
- Elosegui-Artola, A. et al. Force triggers YAP nuclear entry by regulating transport across nuclear pores. *Cell.* 171 (6), 1397-1410 (2017).
- 29. Gudipaty, S. A. et al. Mechanical stretch triggers rapid epithelial cell division through Piezo1. *Nature*. **543** (7643), 118-121 (2017).

- Tang, X. et al. Attenuation of cell mechanosensitivity in colon cancer cells during in vitro metastasis. *PLoS One.* (11), e50443 (2012).
- 31. Cha, C. et al. Top-down synthesis of versatile polyaspartamide linkers for single-step protein conjugation to materials. *Bioconjugate Chemistry.* **22** (12), 2377-2382 (2012).
- 32. Chen, X. et al. Glycosaminoglycans modulate long-range mechanical communication between cells in collagen networks. Proceedings of the National Academy of Sciences of the United States of America. 119 (15), e2116718119 (2022).
- Boyle, J. J., Pless, R. B., Thomopoulos, S., Genin, G.
 M. Direct estimation of surface strain fields from a stereo vision system. *Journal of Biomechanical Engineering*.
 142 (7), 074503 (2020).
- Kim, S., Uroz, M., Bays, J. L., Chen, C. S. Harnessing mechanobiology for tissue engineering. *Developmental Cell.* 56 (2), 180-191 (2021).
- Driscoll, T. P. et al. Cytoskeletal to nuclear strain transfer regulates YAP signaling in mesenchymal stem cells. *Biophysical Journal.* 108 (12), 2783-2793 (2015).
- Guilluy, C. et al. Isolated nuclei adapt to force and reveal a mechanotransduction pathway in the nucleus. *Nature Cell Biology*. 16 (4), 376-381 (2014).
- 37. Vashisth, M. Scaling concepts in 'omics: Nuclear lamin-B scales with tumor growth and often predicts poor prognosis, unlike fibrosis. *Proceedings of the National Academy of Sciences of the United States of America*.
 118 (48), e2112940118 (2021).



- Roberts, A. B. et al. Tumor cell nuclei soften during transendothelial migration. *Journal of Biomechanics*.
 121, 110400 (2021).
- Denais, C. M. et al. Nuclear envelope rupture and repair during cancer cell migration. Science. 352 (6283), 353-358 (2016).
- Raab, M. et al. ESCRT III repairs nuclear envelope ruptures during cell migration to limit DNA damage and cell death. *Science*. 352 (6283), 359-362 (2016).
- Lammerding, J. et al. Lamin A/C deficiency causes defective nuclear mechanics and mechanotransduction. The Journal of Clinical Investigation. 113 (3), 370-378 (2004).
- 42. Shelby, J., Patrick, J., Edgar, S., Chiu, D. T. Monitoring cell survival after extraction of a single subcellular organelle using optical trapping and pulsed-nitrogen laser ablation. *Photochemistry and Photobiology.* **81** (4), 994-1001 (2005).
- Caspi, A., Granek, R., Elbaum, M. Diffusion and directed motion in cellular transport. *Physical Review E.* 66 (1), 011916 (2002).
- 44. Svoboda, K., Block, S. M. Biological applications of optical forces. *Annual Review of Biophysics and Biomolecular Structure.* **23** (1), 247-285 (1994).
- Rohrbach, A. Stiffness of optical traps: quantitative agreement between experiment and electromagnetic theory. *Physical Review Letters*. 95 (16), 168102 (2005).
- Neuman, K. C. et al. Characterization of photodamage to Escherichia coli in optical traps. *Biophysical Journal.* 77 (5), 2856-2863 (1999).

- Kanger, J. S., Subramaniam, V., Driel, R. V. Intracellular manipulation of chromatin using magnetic microbeads. *Chromosome Research.* 16 (3), 511-522 (2008).
- Bausch, A. R. et al. Local measurements of viscoelastic parameters of adherent cell surfaces by magnetic microbead microrheometry. *Biophysical Journal*. **75** (4), 2038-2049 (1998).
- Fisher, J. K. et al. Three-dimensional force microscope: a nanometric optical tracking and magnetic manipulation system for the biomedical sciences. *Review of Scientific Instruments.* 76 (5), 053711 (2005).
- Berret, J. -F. Local viscoelasticity of living cells measured by rotational magnetic spectroscopy. *Nature Communications*. 7, 10134 (2016).
- 51. Hu, B., Dobson, J., El Haj, A. J. Control of smooth muscle α-actin (SMA) up-regulation in HBMSCs using remote magnetic microbead mechano-activation. Nanomedicine: Nanotechnology, Biology and Medicine. 10 (1), 45-55 (2014).
- Kamiyama, D. et al. Versatile protein tagging in cells with split fluorescent protein. *Nature Communications*. 7, 11046 (2016).
- Feng, S. et al. Improved split fluorescent proteins for endogenous protein labeling. *Nature Communications*.
 370 (2017).
- 54. Leonetti, M. D., Sekine, S., Kamiyama, D., Weissman, J. S., Huang, B. A scalable strategy for highthroughput GFP tagging of endogenous human proteins. Proceedings of the National Academy of Sciences of the United States of America. 113 (25), E3501-E3508 (2016).



- Tulpule, A. et al. Kinase-mediated RAS signaling via membraneless cytoplasmic protein granules. *Cell.* 184 (10), 2649-2664 (2021).
- 56. Ansari, A. M. et al. Cellular GFP toxicity and immunogenicity: potential confounders in in vivo cell tracking experiments. Stem Cell Reviews and Reports. 12 (5), 553-559 (2016).
- 57. Gibson, T. J., Seiler, M., Veitia, R. A. The transience of transient overexpression. *Nature Methods.* **10** (8), 715-721 (2013).
- Ratz, M. et al. CRISPR/Cas9-mediated endogenous protein tagging for RESOLFT super-resolution microscopy of living human cells. *Scientific Reports*. 5, 9592 (2015).
- Suzuki, H., Ho, C., Kasagi, N. A chaotic mixer for magnetic microbead-based micro cell sorter. *Journal* of *Microelectromechanical Systems*. 13 (5), 779-790 (2004).
- Luo, Q. et al. All-optical mechanobiology interrogation of yes-associated protein in human cancer and normal cells using a multi-functional system. *Journal of Visualized Experiments*. (178), e62934 (2021).
- Koushki, N. et al. Lamin A redistribution mediated by nuclear deformation determines dynamic localization of YAP. *BioRxiv*. 2020.03.19.998708 (2020).